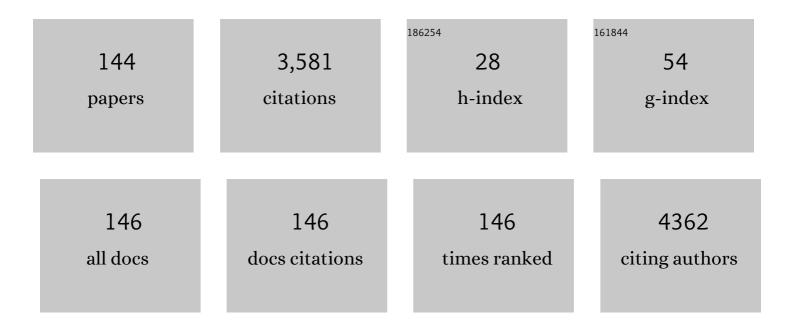
Akio Hiwatashi

List of Publications by Year in descending order

Source: https://exaly.com/author-pdf/191468/publications.pdf Version: 2024-02-01



Δείο Ηινλατλεμι

#	Article	IF	CITATIONS
1	Amide proton transfer imaging of adult diffuse gliomas: correlation with histopathological grades. Neuro-Oncology, 2014, 16, 441-448.	1.2	312
2	Vertebroplasty: cement leakage into the disc increases the risk of new fracture of adjacent vertebral body. American Journal of Neuroradiology, 2004, 25, 175-80.	2.4	299
3	Perfusion Imaging of Brain Tumors Using Arterial Spin-Labeling: Correlation with Histopathologic Vascular Density. American Journal of Neuroradiology, 2008, 29, 688-693.	2.4	210
4	Characterization of IgG4 antiâ€neurofascin 155 antibodyâ€positive polyneuropathy. Annals of Clinical and Translational Neurology, 2015, 2, 960-971.	3.7	148
5	Differentiating primary CNS lymphoma from glioblastoma multiforme: assessment using arterial spin labeling, diffusion-weighted imaging, and 18F-fluorodeoxyglucose positron emission tomography. Neuroradiology, 2013, 55, 135-143.	2.2	110
6	MR Imaging–Based Analysis of Glioblastoma Multiforme: Estimation of <i>IDH1</i> Mutation Status. American Journal of Neuroradiology, 2016, 37, 58-65.	2.4	109
7	Differentiation of high-grade and low-grade diffuse gliomas by intravoxel incoherent motion MR imaging. Neuro-Oncology, 2016, 18, 132-141.	1.2	109
8	Increase in vertebral body height after vertebroplasty. American Journal of Neuroradiology, 2003, 24, 185-9.	2.4	98
9	Grading diffuse gliomas without intense contrast enhancement by amide proton transfer MR imaging: comparisons with diffusion- and perfusion-weighted imaging. European Radiology, 2017, 27, 578-588.	4.5	90
10	Arterial spin labelling at 3-T MR imaging for detection of individuals with Alzheimer's disease. European Radiology, 2009, 19, 2819-2825.	4.5	81
11	3D Turbo Spin-Echo Sequence with Motion-Sensitized Driven-Equilibrium Preparation for Detection of Brain Metastases on 3T MR Imaging. American Journal of Neuroradiology, 2011, 32, 664-670.	2.4	81
12	Kyphoplasty and Vertebroplasty Produce the Same Degree of Height Restoration. American Journal of Neuroradiology, 2009, 30, 669-673.	2.4	78
13	Hypointensity on Diffusion-Weighted MRI of the Brain Related to T2 Shortening and Susceptibility Effects. American Journal of Roentgenology, 2003, 181, 1705-1709.	2.2	69
14	Prevalence and clinicopathological features of H3.3 G34-mutant high-grade gliomas: a retrospective study of 411 consecutive glioma cases in a single institution. Brain Tumor Pathology, 2017, 34, 103-112.	1.7	69
15	Amide proton transfer imaging of brain tumors using a self-corrected 3D fast spin-echo dixon method: Comparison With separate B ₀ correction. Magnetic Resonance in Medicine, 2017, 77, 2272-2279.	3.0	68
16	Kyphoplasty versus Vertebroplasty to Increase Vertebral Body Height: A Cadaveric Study. Radiology, 2005, 237, 1115-1119.	7.3	62
17	Axial loading during MR imaging can influence treatment decision for symptomatic spinal stenosis. American Journal of Neuroradiology, 2004, 25, 170-4.	2.4	53
18	MRI of Glossopharyngeal Neuralgia Caused by Neurovascular Compression. American Journal of Roentgenology, 2008, 191, 578-581.	2.2	52

#	Article	IF	CITATIONS
19	Detection of Middle Ear Cholesteatoma by Diffusion-Weighted MR Imaging: Multishot Echo-Planar Imaging Compared with Single-Shot Echo-Planar Imaging. American Journal of Neuroradiology, 2011, 32, 1915-1918.	2.4	45
20	Cement Leakage During Vertebroplasty Can Be Predicted on Preoperative MRI. American Journal of Roentgenology, 2007, 188, 1089-1093.	2.2	41
21	Scan–rescan reproducibility of parallel transmission based amide proton transfer imaging of brain tumors. Journal of Magnetic Resonance Imaging, 2015, 42, 1346-1353.	3.4	41
22	Ultrahigh-resolution CT scan of the temporal bone. European Archives of Oto-Rhino-Laryngology, 2018, 275, 2797-2803.	1.6	37
23	Patients with Osteoporosis on Steroid Medication Tend to Sustain Subsequent Fractures. American Journal of Neuroradiology, 2007, 28, 1055-1057.	2.4	36
24	Diagnostic utility of intravoxel incoherent motion mr imaging in differentiating primary central nervous system lymphoma from glioblastoma multiforme. Journal of Magnetic Resonance Imaging, 2016, 44, 1256-1261.	3.4	35
25	Evaluation of chronic inflammatory demyelinating polyneuropathy: 3D nerve-sheath signal increased with inked rest-tissue rapid acquisition of relaxation enhancement imaging (3D SHINKEI). European Radiology, 2017, 27, 447-453.	4.5	31
26	Diffusivity of intraorbital lymphoma vs. IgG4-related DISEASE: 3D turbo field echo with diffusion-sensitised driven-equilibrium preparation technique. European Radiology, 2014, 24, 581-586.	4.5	30
27	Amide Proton Transfer Imaging of Diffuse Gliomas: Effect of Saturation Pulse Length in Parallel Transmission-Based Technique. PLoS ONE, 2016, 11, e0155925.	2.5	30
28	Arterial spin labeling of hemangioblastoma: differentiation from metastatic brain tumors based on quantitative blood flow measurement. Neuroradiology, 2012, 54, 809-813.	2.2	29
29	Early strong intrathecal inflammation in cerebellar type multiple system atrophy by cerebrospinal fluid cytokine/chemokine profiles: a case control study. Journal of Neuroinflammation, 2017, 14, 89.	7.2	29
30	Functional connectivity change between posterior cingulate cortex and ventral attention network relates to the impairment of orientation for time in Alzheimer's disease patients. Brain Imaging and Behavior, 2019, 13, 154-161.	2.1	27
31	Early and extensive spinal white matter involvement in neuromyelitis optica. Brain Pathology, 2017, 27, 249-265.	4.1	26
32	Acceleration-selective Arterial Spin-labeling MR Angiography Used to Visualize Distal Cerebral Arteries and Collateral Vessels in Moyamoya Disease. Radiology, 2018, 286, 611-621.	7.3	26
33	Balloon test occlusion of internal carotid artery: Angiographic findings predictive of results. World Journal of Radiology, 2014, 6, 619.	1.1	26
34	Correlation between arterial spin-labeling perfusion and histopathological vascular density of pediatric intracranial tumors. Journal of Neuro-Oncology, 2017, 135, 561-569.	2.9	25
35	Measurement of the perfusion fraction in brain tumors with intravoxel incoherent motion MR imaging: validation with histopathological vascular density in meningiomas. British Journal of Radiology, 2018, 91, 20170912.	2.2	25
36	4D ASL-based MR angiography for visualization of distal arteries and leptomeningeal collateral vessels in moyamoya disease: a comparison of techniques. European Radiology, 2018, 28, 4871-4881.	4.5	25

#	Article	IF	CITATIONS
37	Increased functional connectivity between presupplementary motor area and inferior frontal gyrus associated with the ability of motor response inhibition in obsessive–compulsive disorder. Human Brain Mapping, 2022, 43, 974-984.	3.6	25
38	Pseudolesion in segment II of the liver observed on CT during arterial portography caused by the aberrant left gastric venous drainage. Abdominal Imaging, 1999, 24, 357-359.	2.0	24
39	Quantitative Perfusion Imaging with Pulsed Arterial Spin Labeling: A Phantom Study. Magnetic Resonance in Medical Sciences, 2007, 6, 91-97.	2.0	23
40	Utility of 3â€T FLAIR and 3D short tau inversion recovery MR imaging in the preoperative diagnosis of hippocampal sclerosis: Direct comparison with 1.5â€T FLAIR MR imaging. Epilepsia, 2010, 51, 1820-1828.	5.1	22
41	High-resolution three-dimensional diffusion-weighted MRI/CT image data fusion for cholesteatoma surgical planning: a feasibility study. European Archives of Oto-Rhino-Laryngology, 2015, 272, 3821-3824.	1.6	22
42	Diffusivity of intraorbital lymphoma vs. inflammation: comparison of single shot turbo spin echo and multishot echo planar imaging techniques. European Radiology, 2018, 28, 325-330.	4.5	22
43	Dysfunction between dorsal caudate and salience network associated with impaired cognitive flexibility in obsessive-compulsive disorder: A resting-state fMRI study. NeuroImage: Clinical, 2019, 24, 102004.	2.7	21
44	Clinical significance of <i>CDKN2A</i> homozygous deletion in combination with methylated <i>MGMT</i> status for <i>IDH</i> â€wildtype glioblastoma. Cancer Medicine, 2021, 10, 3177-3187.	2.8	21
45	High-resolution three-dimensional diffusion-weighted imaging of middle ear cholesteatoma at 3.0T MRI: Usefulness of 3D turbo field-echo with diffusion-sensitized driven-equilibrium preparation (TFE–DSDE) compared to single-shot echo-planar imaging. European Journal of Radiology, 2013, 82, e471-e475.	2.6	20
46	Predicting TERT promoter mutation using MR images in patients with wild-type IDH1 glioblastoma. Diagnostic and Interventional Imaging, 2019, 100, 411-419.	3.2	20
47	Vessel-selective 4D-MR angiography using super-selective pseudo-continuous arterial spin labeling may be a useful tool for assessing brain AVM hemodynamics. European Radiology, 2020, 30, 6452-6463.	4.5	20
48	Usefulness of Cone-Beam CT Before and After Percutaneous Vertebroplasty. American Journal of Roentgenology, 2008, 191, 1401-1405.	2.2	19
49	New Vertebral Compression Fractures After Prophylactic Vertebroplasty in Osteoporotic Patients. American Journal of Roentgenology, 2011, 197, 451-456.	2.2	19
50	Diffusion-weighted MR imaging of neuro-Beh�et's disease: a case report. Neuroradiology, 2003, 45, 468-471.	2.2	18
51	Executive Function and Diffusion in Frontal White Matter of Adults with Moyamoya Disease. Journal of Stroke and Cerebrovascular Diseases, 2014, 23, 457-461.	1.6	18
52	Diagnostic accuracy for the epileptogenic zone detection in focal epilepsy could be higher in FDG-PET/MRI than in FDG-PET/CT. European Radiology, 2021, 31, 2915-2922.	4.5	18
53	Lumbar plexus in patients with chronic inflammatory demyelinating polyneuropathy: Evaluation with 3D nerve-sheath signal increased with inked rest-tissue rapid acquisition of relaxation enhancement imaging (3D SHINKEI). European Journal of Radiology, 2017, 93, 95-99.	2.6	17
54	The radiological diagnosis of fenestral otosclerosis: the utility of histogram analysis using multidetector row CT. European Archives of Oto-Rhino-Laryngology, 2014, 271, 3277-3282.	1.6	16

#	Article	IF	CITATIONS
55	A Qualitative and Quantitative Correlation Study of Lumbar Intervertebral Disc Degeneration Using Glycosaminoglycan Chemical Exchange Saturation Transfer, Pfirrmann Grade, and T1-ï• American Journal of Neuroradiology, 2018, 39, 1369-1375.	2.4	16
56	Intravoxel Incoherent Motion MR Imaging of Pediatric Intracranial Tumors: Correlation with Histology and Diagnostic Utility. American Journal of Neuroradiology, 2019, 40, 878-884.	2.4	16
57	Simultaneous MR neurography and apparent T2 mapping in brachial plexus: Evaluation of patients with chronic inflammatory demyelinating polyradiculoneuropathy. Magnetic Resonance Imaging, 2019, 55, 112-117.	1.8	16
58	Spinal cord involvement by atrophy and associations with disability are different between multiple sclerosis and neuromyelitis optica spectrum disorder. European Journal of Neurology, 2020, 27, 92-99.	3.3	16
59	First-line bevacizumab contributes to survival improvement in glioblastoma patients complementary to temozolomide. Journal of Neuro-Oncology, 2020, 146, 451-458.	2.9	16
60	Vertebroplasty for osteoporotic fractures with spinal canal compromise. American Journal of Neuroradiology, 2007, 28, 690-2.	2.4	16
61	A Case of Ecchordosis Physaliphora in the Prepontine Cistern: A Rare Entity in the Differential Diagnosis of an Epidermoid Cyst. World Neurosurgery, 2017, 105, 1033.e11-1033.e14.	1.3	15
62	Contributing Factors in the Pathogenesis of Acquired Cholesteatoma: Size Analysis Based on MDCT. American Journal of Roentgenology, 2011, 196, 1172-1175.	2.2	14
63	Usefulness of perfusion- and diffusion-weighted imaging to differentiate between pilocytic astrocytomas and high-grade gliomas: a multicenter study in Japan. Neuroradiology, 2018, 60, 391-401.	2.2	14
64	Diffusion-weighted magnetic resonance imaging of extraocular muscles in patients with Grave's ophthalmopathy using turbo field echo with diffusion-sensitized driven-equilibrium preparation. Diagnostic and Interventional Imaging, 2018, 99, 457-463.	3.2	14
65	Subsequent Fracture after Percutaneous Vertebroplasty Can Be Predicted on Preoperative Multidetector Row CT. American Journal of Neuroradiology, 2009, 30, 1830-1834.	2.4	13
66	Optimal scan timing for artery–vein separation at whole-brain CT angiography using a 320-row MDCT volume scanner. British Journal of Radiology, 2017, 90, 20160634.	2.2	13
67	HLA-DRB1*04:05 allele is associated with intracortical lesions on three-dimensional double inversion recovery images in Japanese patients with multiple sclerosis. Multiple Sclerosis Journal, 2018, 24, 710-720.	3.0	13
68	Optic, trigeminal, and facial neuropathy related to antiâ€neurofascin 155 antibody. Annals of Clinical and Translational Neurology, 2020, 7, 2297-2309.	3.7	13
69	Disconnection of the right superior parietal lobule from the precuneus is associated with memory impairment in oldest-old Alzheimer's disease patients. Heliyon, 2020, 6, e04516.	3.2	13
70	Alterations of default mode and cingulo-opercular salience network and frontostriatal circuit: A candidate endophenotype of obsessive-compulsive disorder. Progress in Neuro-Psychopharmacology and Biological Psychiatry, 2022, 116, 110516.	4.8	13
71	3D MR Sequence Capable of Simultaneous Image Acquisitions with and without Blood Vessel Suppression: Utility in Diagnosing Brain Metastases. European Radiology, 2015, 25, 901-910.	4.5	12
72	Lumbar plexus in patients with chronic inflammatory demyelinating polyradiculoneuropathy: evaluation with simultaneous <i>T</i> ₂ mapping and neurography method with SHINKEI. British Journal of Radiology, 2018, 91, 20180501.	2.2	12

#	Article	IF	CITATIONS
73	A unique increase in prefrontal gray matter volume in hoarding disorder compared to obsessive-compulsive disorder. PLoS ONE, 2018, 13, e0200814.	2.5	12
74	Differentiation of high-grade from low-grade diffuse gliomas using diffusion-weighted imaging: a comparative study of mono-, bi-, and stretched-exponential diffusion models. Neuroradiology, 2020, 62, 815-823.	2.2	12
75	Aberrant Resting-State Cerebellar-Cerebral Functional Connectivity in Unmedicated Patients With Obsessive-Compulsive Disorder. Frontiers in Psychiatry, 2021, 12, 659616.	2.6	12
76	Evaluation of Diffusivity in the Anterior Lobe of the Pituitary Gland: 3D Turbo Field Echo with Diffusion-Sensitized Driven-Equilibrium Preparation. American Journal of Neuroradiology, 2014, 35, 95-98.	2.4	11
77	Correlations of amide proton transfer-weighted MRI of cerebral infarction with clinico-radiological findings. PLoS ONE, 2020, 15, e0237358.	2.5	11
78	A deep convolutional neural network-based automatic detection of brain metastases with and without blood vessel suppression. European Radiology, 2022, 32, 2998-3005.	4.5	11
79	Cerebral blood flow laterality derived from arterial spin labeling as a biomarker for assessing the disease severity of parkinson's disease. Journal of Magnetic Resonance Imaging, 2017, 45, 1821-1826.	3.4	10
80	Arterial spin-labeling is useful for the diagnosis of residual or recurrent meningiomas. European Radiology, 2018, 28, 4334-4342.	4.5	10
81	Acceleration-selective arterial spin labeling MR angiography for visualization of brain arteriovenous malformations. Neuroradiology, 2019, 61, 979-989.	2.2	10
82	Morphologic Change in Vertebral Body After Percutaneous Vertebroplasty: Follow-Up With MDCT. American Journal of Roentgenology, 2010, 195, W207-W212.	2.2	9
83	Evaluation of glioblastomas and lymphomas with whole-brain CT perfusion: Comparison between a delay-invariant singular-value decomposition algorithm and a Patlak plot. Journal of Neuroradiology, 2016, 43, 266-272.	1.1	9
84	Clinical efficacy of simplified intravoxel incoherent motion imaging using three b-values for differentiating high- and low-grade gliomas. PLoS ONE, 2018, 13, e0209796.	2.5	9
85	Neuroanatomical substrate of chronic psychosis in epilepsy: an MRI study. Brain Imaging and Behavior, 2020, 14, 1382-1387.	2.1	9
86	High Resolution Diffusion-Weighted Imaging for Solitary Orbital Tumors. Clinical Neuroradiology, 2018, 28, 261-266.	1.9	8
87	Prognostic Impact of Tumor Extension in Patients With Advanced Temporal Bone Squamous Cell Carcinoma. Frontiers in Oncology, 2020, 10, 1229.	2.8	8
88	Volumetric study reveals the relationship between outcome and early radiographic response during bevacizumab-containing chemoradiotherapy for unresectable glioblastoma. Journal of Neuro-Oncology, 2021, 154, 187-196.	2.9	8
89	Pure dysarthria and dysarthria-facial paresis syndrome due to internal capsule and/or corona radiata infarction. BMC Neurology, 2015, 15, 184.	1.8	7
90	Primary phosphaturic mesenchymal tumour of the lumbar spine: utility of ⁶⁸ Ga-DOTATOC PET/CT findings. BJR case Reports, 2016, 2, 20150497.	0.2	7

#	Article	IF	CITATIONS
91	Sequential morphological change of Chiari malformation type II following surgical repair of myelomeningocele. Child's Nervous System, 2016, 32, 1069-1078.	1.1	7
92	Evaluation of diffusivity in pituitary adenoma: 3D turbo field echo with diffusion-sensitized driven-equilibrium preparation. British Journal of Radiology, 2016, 89, 20150755.	2.2	7
93	MR Imaging Findings of a Leiomyosarcoma of the Thoracic Spine: A Case Report. Clinical Neuroradiology, 2016, 26, 229-233.	1.9	7
94	Relevance of calcification and contrast enhancement pattern for molecular diagnosis and survival prediction of gliomas based on the 2016 World Health Organization Classification. Clinical Neurology and Neurosurgery, 2019, 187, 105556.	1.4	7
95	Structural changes in Parkinson's disease: voxel-based morphometry and diffusion tensor imaging analyses based on 123I-MIBG uptake. European Radiology, 2017, 27, 5073-5079.	4.5	6
96	Discriminative clinical and neuroimaging features of motor-predominant hereditary diffuse leukoencephalopathy with axonal spheroids and primary progressive multiple sclerosis: A preliminary cross-sectional study. Multiple Sclerosis and Related Disorders, 2019, 31, 22-31.	2.0	6
97	Neurophysiological Face Processing Deficits in Patients With Chronic Schizophrenia: An MEG Study. Frontiers in Psychiatry, 2020, 11, 554844.	2.6	6
98	Vessel-Selective 4D-MRA Using Superselective Pseudocontinuous Arterial Spin-Labeling with Keyhole and View-Sharing for Visualizing Intracranial Dural AVFs. American Journal of Neuroradiology, 2022, 43, 368-375.	2.4	6
99	Ultrashort TE MRI: Usefulness After Percutaneous Vertebroplasty. American Journal of Roentgenology, 2010, 195, W365-W368.	2.2	5
100	3D turbo field echo with diffusion-sensitized driven-equilibrium preparation technique (DSDE-TFE) <i>versus</i> echo planar imaging in evaluation of diffusivity of retinoblastoma. British Journal of Radiology, 2016, 89, 20160074.	2.2	5
101	Lower Hippocampal Volume in Patients with Schizophrenia and Bipolar Disorder: A Quantitative MRI Study. Journal of Personalized Medicine, 2021, 11, 121.	2.5	5
102	High-Resolution STIR for 3-T MRI of the Posterior Fossa: Visualization of the Lower Cranial Nerves and Arteriovenous Structures Related to Neurovascular Compression. American Journal of Roentgenology, 2012, 199, 644-648.	2.2	4
103	Calcium pyrophosphate dihydrate crystal deposition disease of the spinal dura mater: a case report. BJR case Reports, 2018, 4, 20170049.	0.2	4
104	Cerebral syphilitic gumma mimicking glioma: Utility of CT perfusion. Diagnostic and Interventional Imaging, 2018, 99, 755-757.	3.2	4
105	Differences between primary central nervous system lymphoma and glioblastoma: topographic analysis using voxel-based morphometry. Clinical Radiology, 2019, 74, 816.e1-816.e8.	1.1	4
106	Predictive values of early head computed tomography for survival outcome after cardiac arrest in childhood: a pilot study. Scientific Reports, 2021, 11, 12090.	3.3	4
107	Resolution of epidural hematoma related to osteoporotic fracture after percutaneous vertebroplasty. World Journal of Radiology, 2013, 5, 325.	1.1	4
108	Quantitative relaxometry using synthetic MRI could be better than T2-FLAIR mismatch sign for differentiation of IDH-mutant gliomas: a pilot study. Scientific Reports, 2022, 12, .	3.3	4

#	Article	IF	CITATIONS
109	Fractional Anisotropy is Higher in Heschl's Gyrus Than in Superior Temporal Gyrus in Normal Subjects1. Academic Radiology, 2006, 13, 73-76.	2.5	3
110	Additive value of "otosclerosis-weighted―images for the CT diagnosis of fenestral otosclerosis. Acta Radiologica, 2017, 58, 1215-1221.	1.1	3
111	Improved Visualization of Middle Ear Cholesteatoma with Computed Diffusion-weighted Imaging. Magnetic Resonance in Medical Sciences, 2019, 18, 233-237.	2.0	3
112	Contribution of cortical lesions to cognitive impairment in Japanese patients with multiple sclerosis. Scientific Reports, 2020, 10, 5228.	3.3	3
113	Abnormal white matter structure in hoarding disorder. Journal of Psychiatric Research, 2022, 148, 1-8.	3.1	3
114	A case of multiple system atrophy-parkinsonian type with stuttering- and palilalia-like dysfluencies and putaminal atrophy. Journal of Fluency Disorders, 2018, 57, 51-58.	1.7	2
115	A voxel-based analysis of cerebral blood flow abnormalities in obsessive-compulsive disorder using pseudo-continuous arterial spin labeling MRI. PLoS ONE, 2020, 15, e0236512.	2.5	2
116	Gamma distribution model of diffusion MRI for the differentiation of primary central nerve system lymphomas and glioblastomas. PLoS ONE, 2020, 15, e0243839.	2.5	2
117	Alveolar soft part sarcoma of the orbit: A case report. Radiology Case Reports, 2021, 16, 3766-3771.	0.6	2
118	Changes in the Relapse Pattern and Prognosis of Glioblastoma After Approval of First-Line Bevacizumab: A Single-Center Retrospective Study. World Neurosurgery, 2022, 159, e479-e487.	1.3	2
119	Three-dimensional chemical exchange saturation transfer imaging using compressed SENSE for full z-spectrum acquisition. Magnetic Resonance Imaging, 2022, 92, 58-66.	1.8	2
120	Early subsequent fracture after percutaneous vertebroplasty proven by magnetic resonance imaging. European Journal of Radiology Extra, 2008, 68, e93-e95.	0.1	1
121	Spindle cell/sclerosing rhabdomyosarcoma with intracranial invasion without destroying the bone of the skull base: a case report and literature review. Acta Radiologica Open, 2017, 6, 205846011772731.	0.6	1
122	Effectiveness of therapeutic standard concentration barium enema for colonic diverticular bleeding: Preliminary results. European Journal of Radiology Open, 2019, 6, 139-143.	1.6	1
123	Papillary craniopharyngioma coexisting with an intratumoral abscess in a pediatric patient: A case report and review of the literature. Acta Radiologica Open, 2021, 10, 205846012110306.	0.6	1
124	Minute Subsequent Fracture at Prophylactically Treated Adjacent Vertebra After Percutaneous Vertebroplasty. Clinical Neuroradiology, 2014, 24, 381-383.	1.9	0
125	Intravoxel incoherent motion magnetic resonance imaging findings in the acute phase of MELAS : a case report. Brain and Behavior, 2014, 4, 798-800.	2.2	0
126	Metastatic Lung Adenocarcinoma Mimicking Meningioma. Internal Medicine, 2018, 57, 1057-1058.	0.7	0

#	Article	IF	CITATIONS
127	Risk HLA-DRB1 alleles differentially influence brain and lesion volumes in Japanese patients with multiple sclerosis. Journal of the Neurological Sciences, 2020, 413, 116768.	0.6	Ο
128	Brain-sparing cord blood transplantation for the borderline stage of adrenoleukodystrophy. Molecular Genetics and Metabolism Reports, 2021, 28, 100778.	1.1	0
129	Gamma distribution model of diffusion MRI for evaluating the isocitrate dehydrogenase mutation status of glioblastomas. British Journal of Radiology, 2022, 95, 20210392.	2.2	0
130	Title is missing!. , 2020, 15, e0237358.		0
131	Title is missing!. , 2020, 15, e0237358.		Ο
132	Title is missing!. , 2020, 15, e0237358.		0
133	Title is missing!. , 2020, 15, e0237358.		Ο
134	Title is missing!. , 2020, 15, e0237358.		0
135	Title is missing!. , 2020, 15, e0243839.		Ο
136	Title is missing!. , 2020, 15, e0243839.		0
137	Title is missing!. , 2020, 15, e0243839.		Ο
138	Title is missing!. , 2020, 15, e0243839.		0
139	Title is missing!. , 2020, 15, e0243839.		Ο
140	Title is missing!. , 2020, 15, e0243839.		0
141	Title is missing!. , 2020, 15, e0236512.		Ο
142	Title is missing!. , 2020, 15, e0236512.		0
143	Title is missing!. , 2020, 15, e0236512.		0
144	Title is missing!. , 2020, 15, e0236512.		0

9